



Research

Cite this article: Okerblom J, Fletes W, Patel HH, Schenk S, Varki A, Breen EC. 2018 Human-like *Cmah* inactivation in mice increases running endurance and decreases muscle fatigability: implications for human evolution. *Proc. R. Soc. B* **285**: 20181656. <http://dx.doi.org/10.1098/rspb.2018.1656>

Received: 24 July 2018

Accepted: 20 August 2018

Subject Category:

Evolution

Subject Areas:

evolution, physiology, behaviour

Keywords:

human, evolution, running, hunting

Author for correspondence:

Ajit Varki

e-mail: a1varki@ucsd.edu

Electronic supplementary material is available online at <https://dx.doi.org/10.6084/m9.figshare.c.4212719>.

Human-like *Cmah* inactivation in mice increases running endurance and decreases muscle fatigability: implications for human evolution

Jonathan Okerblom^{1,2,3,4}, William Fletes^{2,3,5}, Hemal H. Patel^{6,8}, Simon Schenk⁷, Ajit Varki^{1,2,3,4} and Ellen C. Breen³

¹Center for Academic Research and Training in Anthropogeny (CARTA), ²Glycobiology Research and Training Center (GRTC), ³Department of Medicine, ⁴Department of Cellular and Molecular Medicine, ⁵Initiative for Maximizing Student Development (IMSD) Program, ⁶Department of Anesthesiology, and ⁷Department of Orthopedic Surgery, University of California, San Diego, 9500 Gilman Drive, La Jolla, CA 92093, USA ⁸Veterans Affairs San Diego Healthcare System, 3350 La Jolla Village Drive, San Diego, CA 92161, USA

AV, 0000-0002-2206-975X

Compared to other primates, humans are exceptional long-distance runners, a feature that emerged in genus *Homo* approximately 2 Ma and is classically attributed to anatomical and physiological adaptations such as an enlarged gluteus maximus and improved heat dissipation. However, no underlying genetic changes have currently been defined. Two to three million years ago, an exon deletion in the CMP-Neu5Ac hydroxylase (*CMAH*) gene also became fixed in our ancestral lineage. *Cmah* loss in mice exacerbates disease severity in multiple mouse models for muscular dystrophy, a finding only partially attributed to differences in immune reactivity. We evaluated the exercise capacity of *Cmah*^{-/-} mice and observed an increased performance during forced treadmill testing and after 15 days of voluntary wheel running. *Cmah*^{-/-} hindlimb muscle exhibited more capillaries and a greater fatigue resistance *in situ*. Maximal coupled respiration was also higher in *Cmah* null mice *ex vivo* and relevant differences in metabolic pathways were also noted. Taken together, these data suggest that *CMAH* loss contributes to an improved skeletal muscle capacity for oxygen use. If translatable to humans, *CMAH* loss could have provided a selective advantage for ancestral *Homo* during the transition from forest dwelling to increased resource exploration and hunter/gatherer behaviour in the open savannah.

1. Introduction

Between 2 and 3 Ma, the emergence of genus *Homo* in Africa occurred during a period of transition from forests to increasingly arid landscapes [1–3]. This transition coincided with many postcranial biomechanical adaptations that would have facilitated striding bipedalism and running [4,5]. As descendants of this lineage, humans today rank among the top endurance runners in the animal kingdom [6,7]. Notably, no other extant primate lineage has achieved this distinction [8,9]. Endurance running may have offered *Homo* advantages over other animals less equipped for long distance chases in the open savannah, including the capability for persistence hunting, as well as an increased capacity to exploit larger areas and move across vast landscapes (vagility) [10,11].

The exceptional aerobic capacity of humans exhibited during endurance running has been attributed to major alterations in skeletal biomechanics, as well as to more rapid and efficient heat dissipation, which first emerged in the Old World monkey lineage. The latter phenotype was probably achieved through human loss of fur and a maximal expansion of a vast network of eccrine sweat glands [5,6,12]. Changes in basal metabolic rate, body fat percentage and energy allocation [13], as well as changes in skeletal muscle

physiology and hindlimb muscle volume [14,15] are other key features of likely relevance. However, alternative mutually non-exclusive explanations are possible, and the genetic and molecular events underlying this transition remain unclear.

Two to three million years ago, an *Alu-Alu* genomic fusion caused pseudogenization of the *CMAH* gene [16,17], and this loss of CMP-Neu5Ac hydroxylase (CMAH) function ultimately became fixed within the lineage that eventually gave rise to modern humans [18–20]. CMAH is a hydroxylase/mono-oxygenase enzyme that uses a variety of cofactors, including cytochrome *b5/b5* reductase, iron, oxygen and NADH during the hydroxylation of the *N*-acetyl moiety of the sialic acid *N*-acetylneuraminic acid (Neu5Ac) to convert it to the hydroxylated form, *N*-glycolylneuraminic acid (Neu5Gc) [21]. Initial selection for CMAH loss was possibly owing to pressures from an ancient Neu5Gc-recognizing pathogen [22], and studies of *Cmah*^{-/-} mice with a human-like mutation [23], as well as human and chimpanzee sperm suggest that subsequent fixation in a new lineage might have been due to anti-Neu5Gc antibody-mediated reduction in fertility of null females with wild-type (WT) males [24]. Modelling of such populations suggested a rapid fixation of the null allele, which combined with the timing of approximately 2–3 Ma, allowed us to suggest a role of *Cmah* loss in the divergence of the genus *Homo* [24].

The ramifications of this major change in cell surface biochemistry continue to be explored in mouse models of disease [25], and there is evidence for other significant phenotypic effects, including a human-like increase in sensitivity to certain muscular dystrophy pathologies [26–29]. Although initial muscle studies showed no major differences in the *ex vivo* force frequency relationship between WT and *Cmah* null muscle itself [26,27], independent gene expression studies pointed towards alterations in redox biology [30,31], and several transcription factors (cyclic AMP-responsive element-binding protein 1 (CREB1), CCAAT-enhancer-binding protein β (C/EBP β) and CCAAT-enhancer-binding protein α (C/EBP α)) linked to metabolism and inflammation [26]. Alterations in redox biology associated with *Cmah* loss [30] have also been proposed as a molecular mechanism for age-related hearing loss in *Cmah*^{-/-} mice [23]. However, only limited investigations into the systemic physiological changes in *Cmah*^{-/-} mice have been performed [30–33]. Oxygen delivery and use are particularly important in conditions of maximum aerobic capacity, such as during persistence hunting [34,35]. In this regard, alterations in oxygen delivery have been shown to directly affect maximum aerobic capacity in multiple mammalian model species [36–40]. However, limited studies of the integrative physiology of *Cmah*^{-/-} mice have been performed [30–32]. Considering all of the findings to date, as well as the timing of CMAH loss in relation to fossil evidence for the emergence of the *Homo* running phenotype, we investigated the effects of *Cmah* loss on exercise endurance, via physiological and behavioural comparisons of *Cmah*^{-/-} and WT mice.

2. Material and methods

(a) Animals and tissue collection

All animal experiments were conducted under approved protocols and according to the regulations and guidelines of the Institutional

Animal Care and Use Committee at the University of California, San Diego. An exon deletion identical to the human *CMAH* mutation was generated and bred into a congenic C57BL/6N background as previously described [23]. All WT and *Cmah*^{-/-} animals tested for this study originated from a single founder cage of heterozygous *Cmah* C57BL/6N mice. All terminal tissue collection took place on euthanized mice that were fasted from 9.00 to 13.00, with tissue collection beginning at 13.00.

(b) Treadmill exercise

All mice were familiarized on a treadmill (model no. CL-4, Omnittech, Columbus, OH) for 10 min at a speed of 10 m min⁻¹ for two consecutive days. After walking the mice for 10 min at 10 m min⁻¹, exercise endurance was tested using a treadmill running protocol: speed was increased 1 m min⁻¹ over 10 min, followed by 25 m min⁻¹ for 20 min, 30 m min⁻¹ for 5 min, 35 m min⁻¹ for 5 min, 40 m min⁻¹ for 40 min and then increased at 1 m min⁻¹ until exhaustion. For each running test, exhaustion was defined as the time-point at which the mouse was no longer able to maintain normal running position on the treadmill and/or was sitting on a shock grid (set to less than or equal to 0.1 milliamps) at the rear of the treadmill for four consecutive seconds.

(c) Voluntary exercise

Mice were allowed free access to a running wheel connected to a digital recorder for 15 days. Distance run and average speed were recorded on a daily basis at 9.00. After 15 days of running, running wheels and food were removed at 9.00, and terminal tissue and serum collected from the sacrificed animals after a 4 h fasting period.

(d) *In situ* gastrocnemius fatigue resistance

Fatigue resistance was measured in electrically stimulated gastrocnemius complex (soleus, plantaris and gastrocnemius) as previously described [40]. Mice were anaesthetized with isoflurane and placed on a heated surgery table to maintain temperature (37°C \pm 1) throughout the procedure. Oxygen saturation in the hindlimb was monitored with a Mouse PulseOx (STARR Life Sciences) and maintained above 90% in all groups before experimentation. The sciatic nerve was then exposed and connected to electrodes. The gastrocnemius complex was then separated from the bone, and the tendons connected by a suture to a force transducer (Grass, Astro-Med, West Warwick, RI). The sciatic nerve was electrically stimulated with a Grass S88X Stimulator (Astro-Med, West Warwick, RI) to contract with a single pulse (8 V, 200 ms duration electrical stimulation) to set the optimal muscle length (L_0). To measure fatigue, the gastrocnemius complex was stimulated with repeated trains (8 V, 0.25 trains per second (tps), 80 Hz) until the force generated fell to 60% of the initial force output (time to fatigue).

(e) *Ex vivo* muscle testing

Mice were anaesthetized with isoflurane and the soleus [38] and a strip of the diaphragm with rib attached [41] were dissected. For each test, the muscle was mounted in a chamber filled with Krebs's solution at 32°C (126 mM NaCl, 2.5 mM KCl, 2.5 mM CaCl₂, 1.2 mM MgCl₂, 1.2 mM NaH₂PO₄ and 25 mM NaHCO₃ at pH 7.2) and continuously bubbled with oxygen (95% O₂–5% CO₂). One tendon was tied with silk suture to a force transducer (DMT-USA, Ann Arbor, MI), and the other tendon or rib was tied to an adjustable post at the opposite end of the chamber to allow muscle length to be changed incrementally to set L_0 . Muscles were stimulated with a Grass S88X Stimulator (Astro-Med) at supramaximal voltage using platinum electrodes placed on either side of the muscle. Following 15 min of

equilibration, the muscles were tested for contractile function and fatigue resistance. To assess contractile function, the force frequency relationship was established for each muscle. Maximum isometric tetanic force was measured by recording force output at stimulation frequencies of 1, 15, 30, 50, 80, 100, 150 and 250 Hz (500 ms train duration, monophasic pulses of 0.2 ms duration) for soleus and diaphragm. The muscles were stimulated to contract once every 1.5 min to prevent fatigue. Stability of the muscle was checked by periodically stimulating the muscle at maximal frequency throughout the course of the experiment. To measure fatigue, isometric tetanic contractions were elicited with 500 ms train duration and monophasic pulses of 0.2 ms pulse duration at 80 Hz (soleus) or 40 Hz (diaphragm). Stimulation frequency was increased every 2 min in a progressive manner (the rate of contractions was progressively increased every 2 min starting at a frequency of one every 8 s and changed to one every 4 s to 3 s to 2 s to 1 s over the course of 8 min). Fatigue was defined as the time it took each muscle to reach 60% of the maximal developed force for that muscle. When all testing was finished, L_0 was measured using a reticle with a surgical microscope (Zeiss OPMI, Thornwood, NY), tendons were removed and the muscles were blotted and weighed. Cross-sectional area was calculated as previously described [42], and the specific force was expressed in Newtons per square centimetre.

(f) High-resolution respirometry

Following dissection, soleus and diaphragm tissues were placed immediately in preservation solution at 4°C until measurements could be made (approx. 30 min to 4 h after euthanasia). Preservation medium (BIOPS) contained 10 mM Ca^{2+} EGTA buffer, 20 mM imidazole, 50 mM K^+ -4-morpholineethanesulfonic acid, 0.5 mM dithiothreitol, 6.56 mM MgCl_2 , 5.77 mM ATP, 15 mM phosphocreatine and a pH of 7.1. Tissue samples (approx. 1 mg) were weighed using a microbalance and transferred into a calibrated respirometer (Oxygraph 2 k, Oroboros Instruments, Innsbruck, AT) containing 2 ml of media in each chamber. Respirometry was performed in duplicate at 37°C in stirred media (MiRO5) containing 0.5 mM EGTA, 3 mM MgCl_2 , 60 mM K-lactobionate, 20 mM taurine, 10 mM KH_2PO_4 , 20 mM HEPES, 110 mM sucrose and 1 g l⁻¹ bovine serum albumin essentially fatty acid free, adjusted to pH 7.1. $[\text{O}_2]$ in the media was kept between 300 and 500 pmol ml⁻¹.

A simplified substrate-uncoupler-inhibitor-titration protocol was used to assess maximum ADP-stimulated oxidative phosphorylation (OXPHOS) [43], including 10 mM glutamate and 2 mM malate to support electron entry through complex I (GM; 'LEAK' state), 5 mM ADP to stimulate OXPHOS, 10 mM succinate to maximize convergent electron flux at the Q-junction and 10 μM cytochrome *c* to test for outer mitochondrial membrane integrity as a quality control (greater than 10% cytochrome *c* response was excluded).

(g) Skeletal muscle morphology and immunohistochemistry

Capillaries and fibres in 10 μm cryosections were detected using the Capillary Lead-ATPase method [44]. Images were captured using a Hamamatsu Nanozoomer Slide Scanning System. Total capillary numbers, total fibre numbers and total muscle area were calculated using IMAGEJ software.

(h) Transmission electron microscopy preparation of muscle tissue

Tibialis anterior (TA) tissues were fixed with 2% paraformaldehyde and 2.5% glutaraldehyde in 0.15 M sodium cacodylate

buffer (SC buffer pH 7.4), treated with 1% osmium in 0.15 M sodium cacodylate for 1–2 h on ice, washed with 0.15 M SC buffer followed by rinsing in ddH₂O on ice, incubated in 2% uranyl acetate (UA) for 1 to 2 h at 4°C, dehydrated in ethanol, embedded in durcupan, sectioned by diamond knife and post stained with UA and lead. Images were captured on FEI Spirit Tecnai transmission electron microscopy (TEM) at 80 KV with Eagle 4 k × 4 k camera.

(i) Metabolomics

Metabolomics were performed by the West Coast Metabolomics Center, UC Davis Genome Center-Metabolomics, University of California Davis, 451 Health Sciences Drive, Davis, California 95616, United States *Instrument*: Gerstel CIS4 –with dual MPS Injector/Agilent 6890 GC- Pegasus III TOF MS.

(j) Statistical analysis

Error data represent standard errors of the means (s.e.m.) of the measurements. When comparing WT versus *Cmah*^{-/-}, statistical analysis was performed using two-way analysis of variance (ANOVA) followed by the Tukey's multiple comparisons test or Student's paired two-tailed *t*-test when appropriate. Unless otherwise specified in the figure legend, **p* < 0.05, ***p* < 0.01, ****p* < 0.001 and #*p* < 0.0001 represent estimates of statistical significance.

3. Results

(a) Mice with a human-like *Cmah* deficiency perform better during forced and voluntary exercise testing

Endurance capacity of WT and *Cmah*^{-/-} eight-week-old male mice was tested with a ramp up treadmill running protocol. Separate groups were tested either at baseline or after 30 days of voluntary wheel running. In multiple independent tests, *Cmah*^{-/-} mice displayed approximately 30% greater running endurance compared with WT controls, both at baseline (figure 1a) and after exercise training (figure 1b). A separate study also measured exercise parameters (speed and distance) of eight-week-old WT and *Cmah*^{-/-} male mice during 15 days of voluntary exercise wheel running. After adaptation to exercise training, *Cmah*^{-/-} mice ran at a 12% faster pace (figure 1c) and 20% longer distance per day (figure 1d) compared with WT controls. To determine if any underlying differences in cardiac output or blood haematocrit could be contributing to the observed phenotype, we measured the left ventricular (LV) mass and posterior wall thickness (LVPW) both in diastole and systole by echocardiography. Although we did observe a significant difference in bodyweight in the measured cohort, we did not observe a significant difference in LV mass/bodyweight (*p* = 0.2) or LVPW (*p* = 0.2) in the measured cohort (electronic supplementary material, figure S1A–C). We also quantified the red blood cell (RBC) concentration in blood through complete blood count analysis and did not observe any significant differences in RBC concentrations (electronic supplementary material, figure S1D).

(b) Hindlimb muscles from *Cmah*^{-/-} mice display a greater resistance to fatigue *in situ*

To directly measure fatigue resistance of WT versus *Cmah*^{-/-} mouse muscles with intact vascular and nervous systems, we

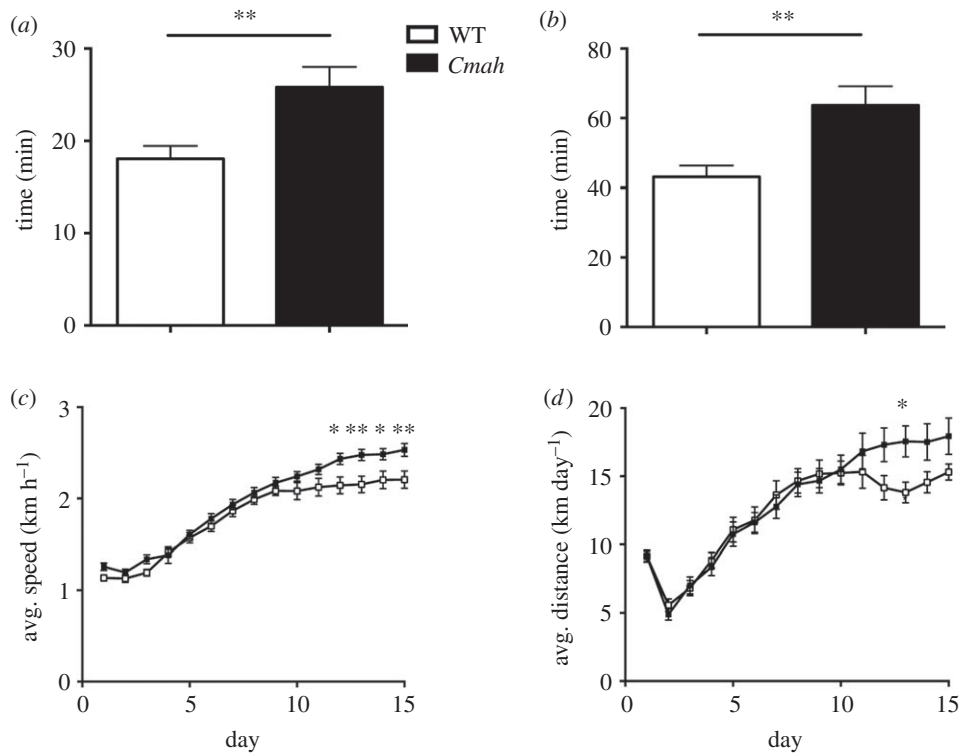


Figure 1. Forced treadmill and voluntary wheel running performance in WT and *Cmah*^{-/-} mice. (a) Untrained endurance times (time to exhaustion) in treadmill running performance ($n = 31$ WT and 36 *Cmah*^{-/-} males, eight weeks of age) and (b) exercise-trained endurance times ($n = 18$ WT and 18 *Cmah*^{-/-}). (c) Average speed and (d) average distance travelled ($n = 18$ WT and 16 *Cmah*^{-/-} males, starting at eight weeks of age) during voluntary exercise with running wheels for two weeks. Error bars are s.e.m. Statistics were determined using two-way ANOVA with Tukey's multiple comparison test. * $p < 0.05$ and ** $p < 0.01$, represent estimates of statistical significance.

electrically stimulated the gastrocnemius complex to contract via the sciatic nerve in anaesthetized mice. The gastrocnemius complex of *Cmah*^{-/-} mice reached fatigue (60% of initial force) at 7 min (7.1 ± 0.4 min) compared to the control group, which took about 3 min (3.2 ± 0.3 min) (figure 2*a,b*). To directly measure the intrinsic fatigue resistance of the muscles *ex vivo*, we evaluated the force frequency (figure 2*c–e*) and time to fatigue (figure 2*f*) of isolated hindlimb (soleus) and respiratory (diaphragm) muscles. Under these *ex vivo* conditions, there were no differences in maximal force (soleus $p = 0.4$, diaphragm $p = 0.8$) or time to fatigue (soleus $p = 0.9$, diaphragm $p = 0.4$) between genotypes. To determine whether vascularity could be a contributing factor to the differences in fatigability between *in situ* and *ex vivo* contractions, we analysed the capillary per fibre ratio of a primarily oxidative (soleus) and glycolytic (plantaris) muscles of the hindlimb. Histological analysis of WT versus *Cmah*^{-/-} hindlimb muscles demonstrated that the capillary to fibre ratio was significantly higher in the red oxidative muscle (soleus) but not the white glycolytic muscle (plantaris) in non-exercise-trained *Cmah*^{-/-} mice versus WT controls (figure 3*a*). To determine the mitochondrial content, we analysed the mitochondrial volume density of a glycolytic hindlimb muscle (TA) by electron microscopy and did not observe a significant difference ($p = 0.4$, figure 3*b*). We also checked the citrate synthase activity of four different muscles (heart, diaphragm, gastrocnemius and soleus) and observed a trend towards an elevated citrate synthase activity in *Cmah*^{-/-} versus WT mice ($p = 0.07$, electronic supplementary material, figure S2*A*). When performing individual comparisons, we did observe a significant difference in the diaphragm (* $p = 0.03$, electronic supplementary material, figure S2*A*).

(c) Locomotor and respiratory fibres from *Cmah*^{-/-} mice show a greater maximal mitochondrial capacity

To assess the coupled respiratory capacity of WT and *Cmah*^{-/-} myofibre, oxygen consumption (O_2 flux) was measured in permeabilized fibre bundles derived from diaphragm (figure 3*c*) and soleus (figure 3*d*) in the presence of complex I substrates (glutamate and malate), state III (saturating ADP conditions) and complex I + II substrates while in state III (glutamate + malate + ADP + succinate) with subsequent cytochrome *c* addition as a quality control. We found that under saturating conditions of ADP and mitochondrial complex I + II substrates, *Cmah*^{-/-} muscle had a greater O_2 flux (oxygen consumption per second normalized to muscle fibre bundle mass) compared with WT controls (figure 3*c,d*), indicating a higher maximum ADP-stimulated OXPHOS capacity in *Cmah*^{-/-} mouse myofibres compared with WT controls in conditions where the cytochrome *c* response (as a marker of mitochondrial outer membrane damage) was very minimal (average $< 1\%$). To determine oxygen substrate use, we also measured the K_m ($p50$) of oxygen in isolated mitochondria from heart and gastrocnemius and did not observe a significant difference ($p = 0.31$, electronic supplementary material, figure S2*B*).

(d) Amino acid metabolism and pentose phosphate pathway metabolites are enriched in *Cmah*^{-/-} exercise-trained mouse locomotor muscle

To explore differences in major metabolic pathways, the soleus from exercised and non-exercised WT and

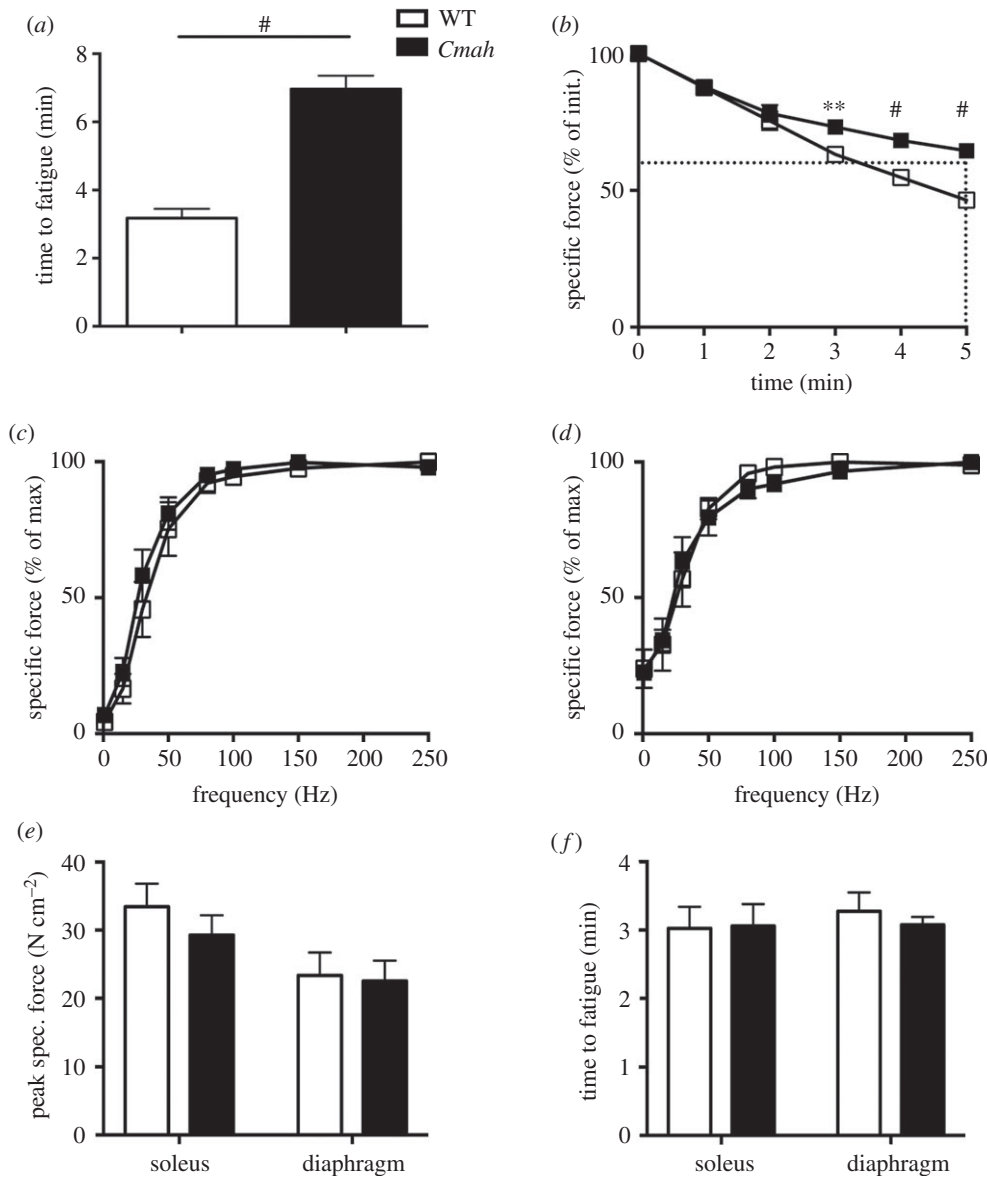


Figure 2. Hindlimb and respiratory muscle contractile function in WT and *Cmah*^{-/-} mice. (a) Time to fatigue (60% of initial) of gastrocnemius complex electrically stimulated via the sciatic nerve ($n = 6$). (b) Force production of the gastrocnemius complex normalized to per cent of initial contraction during the first 5 min ($n = 6$) of tetanic contractions. Dotted line represents time to fatigue (60% of initial contraction) (c) Force frequency relationship of soleus ($n = 4$) and (d) diaphragm ($n = 4$). (e) Peak specific forces in soleus and diaphragm during force frequency testing and (f) time to fatigue (60% of initial) during repetitive tetanic contractions in soleus (80 Hz) and diaphragm (40 Hz). Error bars are s.e.m. Statistics were determined using two-way ANOVA with Tukey's multiple comparison test. ** $p < 0.01$ and # $p < 0.0001$ represent estimates of statistical significance.

Cmah^{-/-} mice was subjected to untargeted GC-TOF metabolomics analysis. The top 100 metabolites showing differences are visually illustrated by a heat map (figure 4). Targeted evaluation of specific metabolites illustrates a greater abundance of multiple amino acids in *Cmah*^{-/-} exercise-trained muscle compared with WT exercised trained muscle, particularly proline, phenylalanine and the branched chain amino acids (BCAAs) leucine and isoleucine. Aspartate, threonine, asparagine and tyrosine were also upregulated in *Cmah*^{-/-} exercise-trained soleus but not in WT exercise-trained soleus in the same conditions. Several other amino acids were upregulated in both WT and *Cmah*^{-/-} exercised tissues as a general effect of exercise shared between the two groups, although most were trending towards higher upregulation in *Cmah*^{-/-} exercised muscle versus WT exercised muscle (figure 4). Multiple metabolites in the pentose phosphate pathway such as ribulose-5-phosphate, ribose and xylulose

were also upregulated in *Cmah*^{-/-} exercise-trained soleus compared to WT controls (figure 4).

4. Discussion and conclusion

Hominin evolution is like a bush, with many lineages of hominins coexisting throughout much of the past 6 Myr [45,46]. While hominin bipedalism emerged early and possibly more than once, *CMAH* loss [19,20] occurred later and roughly coincides with the major biomechanical and environmental changes that took place as hominins probably transitioned to a more carnivorous diet [1–3,47]. Such a transition could have been greatly facilitated by an increase in the capabilities of ancient hominins to perform persistence hunting and explore a wider range for resources. For this reason, the exact timing of *CMAH* loss in the fossil record is of interest, and a method to measure a stable Neu5Gc metabolite in 4 Myr-old fossil material has recently been developed [48].

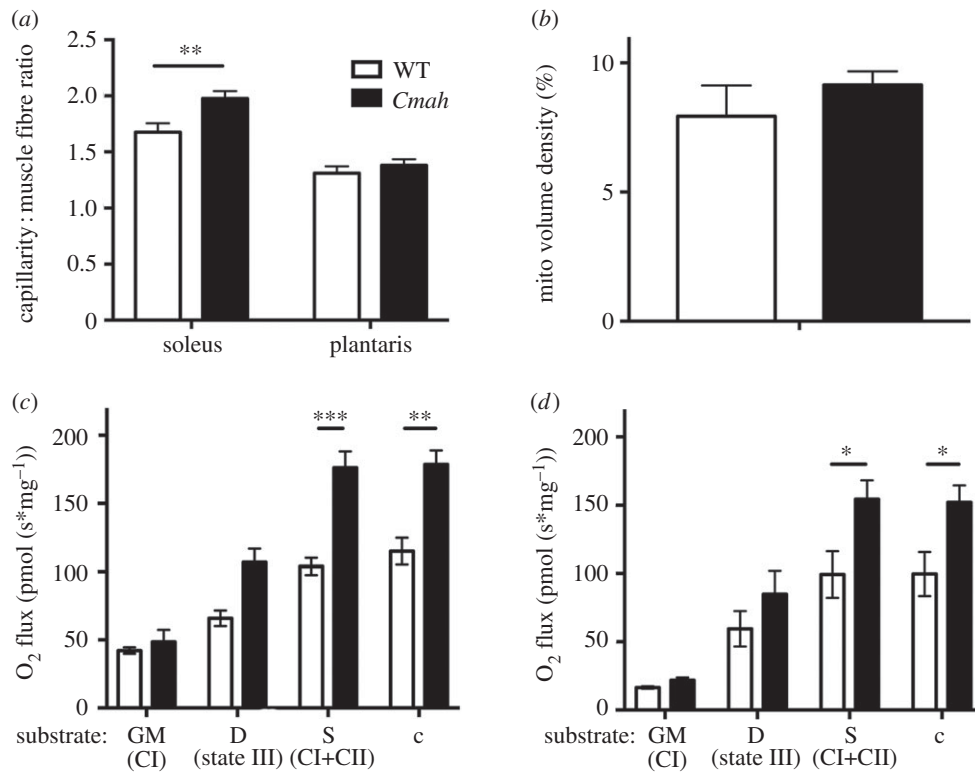


Figure 3. Skeletal muscle vascularity and mitochondrial respiration in WT and *Cmah*^{-/-} mice. (a) Muscle capillary-to-fibre ratio was measured by lead ATPase stain in the soleus ($n = 6$) and plantaris ($n = 5$). (b) Mitochondrial volume density was also measured by transmission electron microscopy (TEM) of the tibialis anterior ($n = 3$). (c) Diaphragm ($n = 4$ WT and 6 *Cmah*^{-/-}) and (d) soleus ($n = 6$) saponin-permeabilized muscle fibre bundles were exposed to saturating conditions of the following substrates: glutamate and malate (GM) to measure complex I respiration, ADP to measure state III respiration, complex II substrate succinate (Suc) to measure complex I and complex II respiration combined and cytochrome *c* (Cyt *c*) as a quality control to ensure mitochondrial outer membrane integrity. Error bars are s.e.m. Statistics were determined using two-way ANOVA with Tukey's multiple comparison test. * $p < 0.05$, ** $p < 0.01$ and *** $p < 0.001$ represent estimates of statistical significance.

Emulating human *CMAH* loss in mice generates an increased capability to use oxygen. This is most evident by an increase in endurance running performance, muscle fatigue resistance *in situ* and myofibre respiration *ex vivo*. Importantly, these differences appear to be completely independent of differences in biomechanics or eccrine sweat glands already associated with the success of humans for long distance running compared with other vertebrates [5]. At least part of this difference in oxygen use could be owing to a difference in baseline skeletal muscle capillarity. This was observed in the more oxidative soleus but not the more glycolytic plantaris. Notably, the soleus is a highly oxidative slow twitch muscle compared with most muscles in a mouse and more closely resembles the type 1 and type 2A fibre type distribution prevalent in humans and other relatively large mammals [49,50]. Compared to other primates, human muscle also contains a greater proportion of myosin heavy chain I (MHC I) fibres [15,51] and likely associated capillaries, another predictor of human endurance [52]. Increasing the number of capillaries supplying each myofibre increases vital nutrient and oxygen availability to mitochondria during periods of prolonged endurance exercise or providing resistance to muscle fatigue as we measured *in situ* [38,40,53–56]. In this regard, a comparable performance of muscle fatigability *ex vivo* further strengthens the hypothesis that greater oxygen availability contributes to the superior muscle fatigue resistance measured *in situ* in mice with *Cmah* loss [57–59]. This is supported by the technical limitation in detecting small differences in O₂ use *ex vivo*

owing to the known diffusion limitations in isolated muscles externally bathed in an O₂-saturating solution [60]. The observed increase in ADP-stimulated OXPHOS of saponin-permeabilized muscle fibre bundles, however, does suggest that *Cmah*^{-/-} myofibres have a higher capacity to use O₂.

The heat map of metabolites illustrates a major effect of exercise adaptation on the muscle metabolite profile. Although there is no significant difference in the citric acid cycle metabolites measured (citrate, malate and succinate) between WT and *Cmah*^{-/-} exercise-adapted mice, greater increases in anabolic amino acids such as the BCAAs, leucine and isoleucine, were observed in *Cmah*^{-/-} exercised muscle. In addition to their anabolic effects after physical exercise [61], increased muscle BCAA can also prevent oxidative damage and enhance physical endurance in mice [62]. The higher prevalence of metabolites of the anabolic pentose phosphate pathway in *Cmah*^{-/-} exercised mice could also help to combat oxidative stress [63–66].

One of the disparate clues that lead us to test endurance capacity in *Cmah*^{-/-} mice was the finding that when crossing this genotype into the human-like Duchenne Muscular Dystrophy mouse model (mdx), *Cmah*^{-/-}/mdx mice display a much more severe and human-like muscular dystrophy pathology [26,27]. The C/EBP family of transcription factors connect changes associated with metabolism [67] to the inflammatory response [68,69] and muscle wasting [70]. We have previously shown that the family member (C/EBP β) could be modulated simply by causing uptake and metabolic incorporation of Neu5Gc into macrophages *ex vivo* [29] and

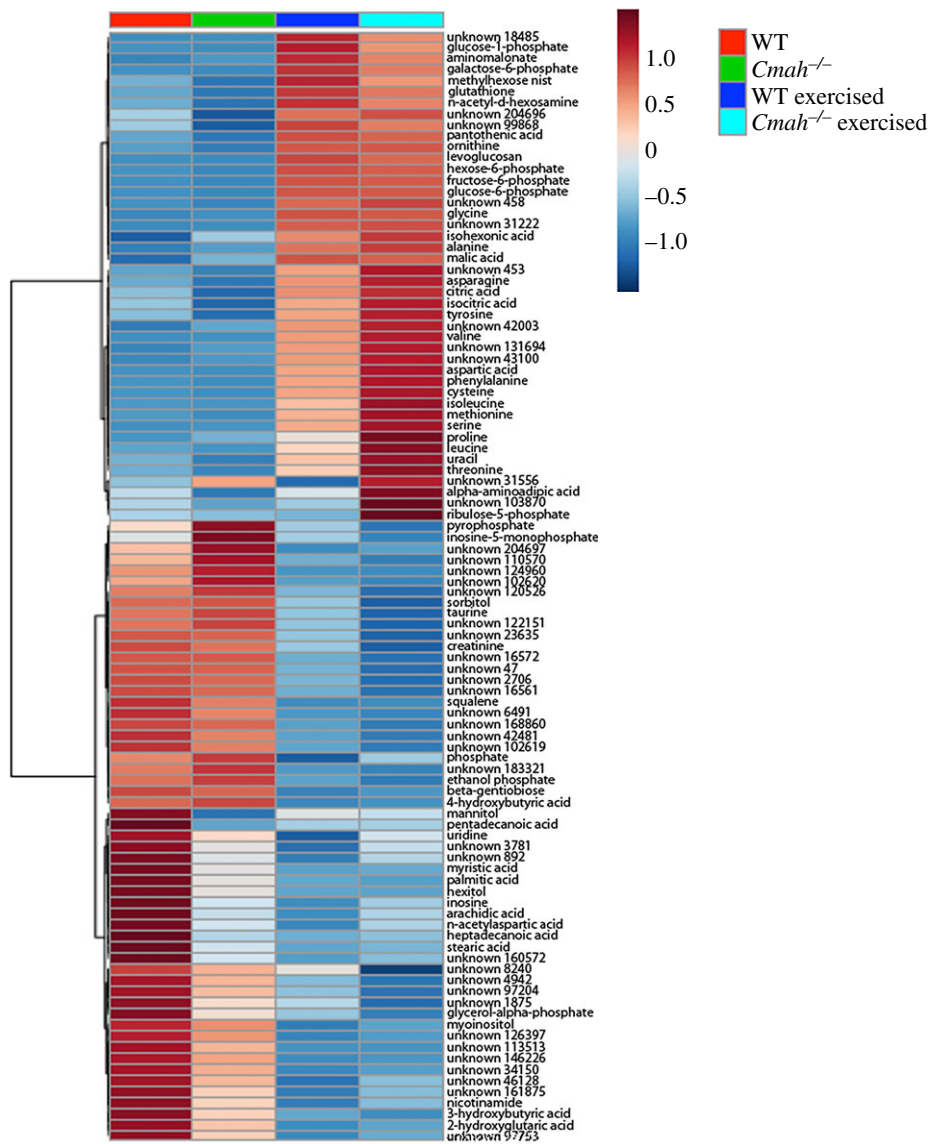


Figure 4. Metabolite profiles in WT versus *Cmah*^{-/-} mice. Heat map for visualization of the average value per group of the 100 most significant metabolites from the soleus muscles of non-exercised ($n = 10$ WT and 7 *Cmah*^{-/-}) and exercise-trained ($n = 13$ WT and 12 *Cmah*^{-/-}) mice determined by one-way ANOVA.

that C/EBP β was differentially expressed in WT versus *Cmah*^{-/-} macrophages. Alterations in macrophage C/EBP β expression or activity during the development and/or polarization of macrophages could be a contributing factor towards the differences in baseline capillary to muscle fibre ratios observed in the soleus muscles of *Cmah*^{-/-} mice [71]. Previously reported genechip analysis revealed that the expression of another C/EBP family member (C/EBP δ) and the transcriptional activity of CREB1 are upregulated in *Cmah*^{-/-} gastrocnemius muscle compared to WT controls [26].

The single oxygen atom added to Neu5Ac by CMAH generates Neu5Gc, and this conversion from an acetyl group to a glycolyl group probably alters the amphipathicity and/or charge of the primary sugar molecule as well as the macromolecules carrying them at the membrane surface. We believe that surface Neu5Gc loss could increase membrane surface hydrophobicity, which could facilitate a greater oxygen diffusion rate, but this is difficult to test. On the other hand, the intracellular turnover of these sialic acids would generate acetate and glycolate, respectively, which could intrinsically alter cellular metabolic flux. Sialic acid-binding proteins and sialidases can also differentiate

between the two types of chemical structures. Given that the great majority of self-surface and secreted molecules of all cell types (including muscle) express such sialic acids (often at high densities), the loss of Neu5Gc (and the resulting excess of Neu5Ac) in the hominin lineage is likely to have had multiple effects on multiple pathways and systems. Thus, there are many mechanisms possible and we have only begun to explore some of them. Our current work suggests that there were probably complex multilevel effects of *Cmah* loss on skeletal muscle and vascular physiology during the evolution of hominins. Integrated changes in the O₂ transport system provide a greater capability for long distance running *in vivo*, resistance to muscle fatigability *in situ* and greater maximal ADP-stimulated OXPHOS in skeletal muscle, despite no measurable difference in fatigue resistance *ex vivo*. These data suggest a critical role for oxygen delivery and use in the muscle endurance phenotype.

Given that Neu5Gc loss altered the surfaces of almost all cells in the body, it is not surprising that no single mechanism can fully account for the increase in spontaneous exercise and maximal endurance observed in *Cmah*^{-/-} mice. Further study of all components of the integrated oxygen transport

system, including cardiac function, are needed. For the time being, given the timing of the mutation and the potential relevance of its fixation to the emergence of the genus *Homo*, it is reasonable to speculate that this mutation may have been essential for running faster and further. Thus, the emergence of an endurance phenotype critical to our ancestral lineage: an increased range for resource exploration and the ability to chase down prey over long distances.

Ethics. All animal experiments were conducted under approved protocols of the Institutional Animal Care and Use Committee at the University of California, San Diego.

References

- deMenocal PB. 2011 Anthropology. Climate and human evolution. *Science* **331**, 540–542 (doi:10.1126/science.1190683)
- White TD, Suwa G, Hart WK, Walter RC, WoldeGabriel G, de Heinzelin J, Clark JD, Asfaw B, Vrba E. 1993 New discoveries of *Australopithecus* at Maka in Ethiopia. *Nature* **366**, 261–265. (doi:10.1038/366261a0)
- Semaw S, Renne P, Harris JW, Feibel CS, Bernor RL, Fesseha N, Mowbray K. 1997 2.5-million-year-old stone tools from Gona, Ethiopia. *Nature* **385**, 333–336. (doi:10.1038/385333a0)
- Bramble DM, Lieberman DE. 2004 Endurance running and the evolution of *Homo*. *Nature* **432**, 345–352. (doi:10.1038/nature03052)
- Lieberman DE. 2015 Human locomotion and heat loss: an evolutionary perspective. *Compr. Physiol.* **5**, 99–117. (doi:10.1002/cphy.c140011)
- Carrier DR, Kapoor AK, Kimura T, Nickels MK, Scott EC, So JK, Trinkaus E. 1984 The energetic paradox of human running and hominid evolution [and comments and reply]. *Curr. Anthropol.* **25**, 483–495. (doi:10.1086/203165)
- Lieberman DE, Bramble DM. 2007 The evolution of marathon running: capabilities in humans. *Sports Med.* **37**, 288–290. (doi:10.2165/00007256-200737040-00004)
- Sockol MD, Raichlen DA, Pontzer H. 2007 Chimpanzee locomotor energetics and the origin of human bipedalism. *Proc. Natl Acad. Sci. USA* **104**, 12 265–12 269 (doi:10.1073/pnas.0703267104).
- Pontzer H, Raichlen DA, Rodman PS. 2014 Bipedal and quadrupedal locomotion in chimpanzees. *J. Hum. Evol.* **66**, 64–82. (doi:10.1016/j.jhevol.2013.10.002)
- Lieberman DE, Bramble DM, Raichlen DA, Shea JJ. 2007 The evolution of endurance running and the tyranny of ethnography: a reply to Pickering and Bunn (2007). *J. Hum. Evol.* **53**, 439–442 (doi:10.1016/j.jhevol.2007.07.002)
- Liebenberg L. 2008 The relevance of persistence hunting to human evolution. *J. Hum. Evol.* **55**, 1156–1159. (doi:10.1016/j.jhevol.2008.07.004)
- Best A, Kamilar JM. 2018 The evolution of eccrine sweat glands in human and nonhuman primates. *J. Hum. Evol.* **117**, 33–43. (doi:10.1016/j.jhevol.2017.12.003)
- Pontzer H *et al.* 2016 Metabolic acceleration and the evolution of human brain size and life history. *Nature* **533**, 390–392. (doi:10.1038/nature17654)
- Pontzer H. 2017 Economy and endurance in human evolution. *Curr. Biol.* **27**, R613–R621. (doi:10.1016/j.cub.2017.05.031)
- O'Neill MC, Umberger BR, Holowka NB, Larson SG, Reiser PJ. 2017 Chimpanzee super strength and human skeletal muscle evolution. *Proc. Natl Acad. Sci. USA* **114**, 7343–7348. (doi:10.1073/pnas.1619071114)
- Irie A, Koyama S, Kozutsumi Y, Kawasaki T, Suzuki A. 1998 The molecular basis for the absence of N-glycolylneuraminic acid in humans. *J. Biol. Chem.* **273**, 15 866–15 871. (doi:10.1074/jbc.273.25.15866)
- Chou HH *et al.* 1998 A mutation in human CMP-sialic acid hydroxylase occurred after the *Homo-Pan* divergence. *Proc. Natl Acad. Sci. USA* **95**, 11 751–11 756. (doi:10.1073/pnas.95.20.11751)
- Hayakawa T, Satta Y, Gagneux P, Varki A, Takahata N. 2001 Alu-mediated inactivation of the human CMP-N-acetylneuraminic acid hydroxylase gene. *Proc. Natl Acad. Sci. USA* **98**, 11 399–11 404. (doi:10.1073/pnas.191268198)
- Chou HH *et al.* 2002 Inactivation of CMP-N-acetylneuraminic acid hydroxylase occurred prior to brain expansion during human evolution. *Proc. Natl Acad. Sci. USA* **99**, 11 736–11 741. (doi:10.1073/pnas.182257399)
- Hayakawa T, Aki I, Varki A, Satta Y, Takahata N. 2006 Fixation of the human-specific CMP-N-acetylneuraminic acid hydroxylase pseudogene and implications of haplotype diversity for human evolution. *Genetics* **172**, 1139–1146. (doi:10.1534/genetics.105.046995)
- Varki A, Schnaar RL, Schauer R. 2017 Sialic acids and other nonulosonic acids. In *Essentials of glycobiology* (eds AVarki *et al.*), pp. 179–195. Cold Spring Harbor, NY: Cold Spring Harbor Laboratory Press.
- Varki A, Gagneux P. 2009 Human-specific evolution of sialic acid targets: explaining the malignant malaria mystery. *Proc. Natl Acad. Sci. USA* **106**, 14 739–14 740. (doi:10.1073/pnas.0908196106)
- Hedlund M *et al.* 2007 N-glycolylneuraminic acid deficiency in mice: implications for human biology and evolution. *Mol. Cell. Biol.* **27**, 4340–4346. (doi:10.1128/MCB.00379-07)
- Ghaderi D, Springer SA, Ma F, Cohen M, Secret P, Taylor RE, Varki A, Gagneux P. 2011 Sexual selection by female immunity against paternal antigens can fix loss of function alleles. *Proc. Natl Acad. Sci. USA* **108**, 17 743–17 748. (doi:10.1073/pnas.1102302108)
- Okerblom J, Varki A. 2017 Biochemical, cellular, physiological, and pathological consequences of human loss of N-glycolylneuraminic acid. *Chembiochem* **18**, 1155–1171. (doi:10.1002/cbic.201700077)
- Chandrasekharan K, Yoon JH, Xu Y, deVries S, Camboni M, Janssen PM, Varki A, Martin PT. 2010 A human-specific deletion in mouse *Cmah* increases disease severity in the *mdx* model of Duchenne muscular dystrophy. *Sci. Transl. Med.* **2**, 42ra54. (doi:10.1126/scitranslmed.3000692)
- Martin PT, Camboni M, Xu R, Golden B, Chandrasekharan K, Wang CM, Varki A, Janssen PM. 2013 N-glycolylneuraminic acid deficiency worsens cardiac and skeletal muscle pathophysiology in α -sarcoglycan-deficient mice. *Glycobiology* **28**, 833–843. (doi:10.1093/glycob/cwt020)
- Martin PT, Golden B, Okerblom J, Camboni M, Chandrasekharan K, Xu R, Varki A, Flanigan KM, Kornegay JN. 2014 A comparative study of N-glycolylneuraminic acid (Neu5Gc) and cytotoxic T cell (CT) carbohydrate expression in normal and dystrophin-deficient dog and human skeletal muscle. *PLoS ONE* **9**, e88226. (doi:10.1371/journal.pone.0088226)
- Okerblom JJ, Schwarz F, Olson J, Fletes W, Ali SR, Martin PT, Glass CK, Nizet V, Varki A. 2017 Loss of CMAH during human evolution primed the monocyte-macrophage lineage toward a more inflammatory and phagocytic state. *J. Immunol.* **198**, 2366–2373. (doi:10.4049/jimmunol.1601471)
- Kwon DN, Park WJ, Choi YJ, Gurunathan S, Kim JH. 2015 Oxidative stress and ROS metabolism via

- down-regulation of siruin 3 expression in Cmah-null mice affect hearing loss. *Aging (Albany NY)* **7**, 579–594. (doi:10.18632/aging.100800)
31. Kwon DN, Choi YJ, Cho SG, Park C, Seo HG, Song H, Kim JH. 2015 CMP-Neu5Ac hydroxylase null mice as a model for studying metabolic disorders caused by the evolutionary loss of Neu5Gc in humans. *BioMed. Res. Int.* **2015**, 1–16. (doi:10.1155/2015/830315)
 32. Kavalier S, Morinaga H, Jih A, Fan W, Hedlund M, Varki A, Kim JJ. 2011 Pancreatic beta-cell failure in obese mice with human-like CMP-Neu5Ac hydroxylase deficiency. *FASEB J.* **25**, 1887–1893. (doi:10.1096/fj.10-175281)
 33. Kwon DN, Chang BS, Kim JH. 2014 Gene expression and pathway analysis of effects of the CMAH deactivation on mouse lung, kidney and heart. *PLoS ONE* **9**, e107559. (doi:10.1371/journal.pone.0107559)
 34. Roca J, Hogan MC, Story D, Bebout DE, Haab P, Gonzalez R, Ueno O, Wagner PD. 1989 Evidence for tissue diffusion limitation of VO₂max in normal humans. *J. Appl. Physiol.* **67**, 291–299. (doi:10.1152/jappl.1989.67.1.291)
 35. Richardson RS, Grassi B, Gavin TP, Haseler LJ, Tagore K, Roca J, Wagner PD. 1999 Evidence of O₂ supply-dependent VO₂ max in the exercise-trained human quadriceps. *J. Appl. Physiol.* **86**, 1048–1053. (doi:10.1152/jappl.1999.86.3.1048)
 36. Richardson RS, Leigh JS, Wagner PD, Noyszewski EA. 1999 Cellular PO₂ as a determinant of maximal mitochondrial O₂ consumption in trained human skeletal muscle. *J. Appl. Physiol.* **87**, 325–331. (doi:10.1152/jappl.1999.87.1.325)
 37. Koga S, Rossiter HB, Heinonen I, Musch TI, Poole DC. 2014 Dynamic heterogeneity of exercising muscle blood flow and O₂ utilization. *Med. Sci. Sports Exerc.* **46**, 860–876. (doi:10.1249/MSS.000000000000178)
 38. Delavar H, Nogueira L, Wagner PD, Hogan MC, Metzger D, Breen EC. 2014 Skeletal myofiber VEGF is essential for the exercise training response in adult mice. *Am. J. Physiol. Regul. Integr. Comp. Physiol.* **306**, R586–R595. (doi:10.1152/ajpregu.00522.2013)
 39. Tang K, Gu Y, Dalton ND, Wagner H, Peterson KL, Wagner PD, Breen EC. 2016 Selective life-long skeletal myofiber-targeted VEGF gene ablation impairs exercise capacity in adult mice. *J. Cell. Physiol.* **231**, 505–511. (doi:10.1002/jcp.25097)
 40. Knapp AE, Goldberg D, Delavar H, Trisko BM, Tang K, Hogan MC, Wagner PD, Breen EC. 2016 Skeletal myofiber VEGF regulates contraction-induced perfusion and exercise capacity but not muscle capillarity in adult mice. *Am. J. Physiol. Regul. Integr. Comp. Physiol.* **311**, R192–R199. (doi:10.1152/ajpregu.00533.2015)
 41. Mangner N *et al.* 2016 Exercise training prevents diaphragm contractile dysfunction in heart failure. *Med. Sci. Sports Exerc.* **48**, 2118–2124. (doi:10.1249/MSS.0000000000001016)
 42. Close RI. 1972 Dynamic properties of mammalian skeletal muscles. *Physiol. Rev.* **52**, 129–197. (doi:10.1152/physrev.1972.52.1.129)
 43. Pesta D, Gnaiger E. 2012 High-resolution respirometry: OXPHOS protocols for human cells and permeabilized fibers from small biopsies of human muscle. *Methods Mol. Biol.* **810**, 25–58. (doi:10.1007/978-1-61779-382-0_3)
 44. Rosenblatt JD, Kuzon WM, Pyley MJ, Pynn BR, McKee NH. 1987 A histochemical method for the simultaneous demonstration of capillaries and fiber type in skeletal muscle. *Stain Technol.* **62**, 85–92. (doi:10.3109/10520298709107973)
 45. Wood B, Richmond BG. 2000 Human evolution: taxonomy and paleobiology. *J. Anat.* **197**, 19–60. (doi:10.1046/j.1469-7580.2000.19710019.x)
 46. Wood B, Boyle EK. 2016 Hominin taxic diversity: fact or fantasy. *Am. J. Phys. Anthropol.* **159**, S37–S78. (doi:10.1002/ajpa.22902)
 47. Cerling TE *et al.* 2011 Woody cover and hominin environments in the past 6 million years. *Nature* **476**, 51–56. (doi:10.1038/nature10306)
 48. Bergfeld AK, Lawrence R, Diaz SL, Pearce OMT, Ghaderi D, Gagneau P, Leakey MG, Varki A. 2017 N-glycolyl groups of nonhuman chondroitin sulfates survive in ancient fossils. *Proc. Natl Acad. Sci. USA* **114**, E8155–E8164. (doi:10.1073/pnas.1706306114)
 49. Schiaffino S, Reggiani C. 2011 Fiber types in mammalian skeletal muscles. *Physiol. Rev.* **91**, 1447–1531. (doi:10.1152/physrev.00031.2010)
 50. Tirrell TF, Cook MS, Carr JA, Lin E, Ward SR, Lieber RL. 2012 Human skeletal muscle biochemical diversity. *J. Exp. Biol.* **215**, 2551–2559. (doi:10.1242/jeb.069385)
 51. Myatt JP, Schilling N, Thorpe SK. 2011 Distribution patterns of fibre types in the triceps surae muscle group of chimpanzees and orangutans. *J. Anat.* **218**, 402–412. (doi:10.1111/j.1469-7580.2010.01338.x)
 52. Coyle EF. 1995 Integration of the physiological factors determining endurance performance ability. *Exerc. Sport Sci. Rev.* **23**, 25–63. (doi:10.1249/00003677-199500230-00004)
 53. Andersen P, Henriksson J. 1977 Capillary supply of the quadriceps femoris muscle of man: adaptive response to exercise. *J. Physiol.* **270**, 677–690. (doi:10.1113/jphysiol.1977.sp011975)
 54. Ingjer F. 1978 Maximal aerobic power related to the capillary supply of the quadriceps femoris muscle in man. *Acta Physiol. Scand.* **104**, 238–240. (doi:10.1111/j.1748-1716.1978.tb06273.x)
 55. Poole DC, Mathieu-Costello O. 1996 Relationship between fiber capillarization and mitochondrial volume density in control and trained rat soleus and plantaris muscles. *Microcirculation* **3**, 175–186. (doi:10.3109/10739689609148286)
 56. Olfert IM, Howlett RA, Tang K, Dalton ND, Gu Y, Peterson KL, Wagner PD, Breen EC. 2009 Muscle-specific VEGF deficiency greatly reduces exercise endurance in mice. *J. Physiol.* **587**, 1755–1767. (doi:10.1113/jphysiol.2008.164384)
 57. Poole DC, Copp SW, Hirai DM, Musch TI. 2011 Dynamics of muscle microcirculatory and blood-myocyte O₂ flux during contractions. *Acta Physiol. (Oxf.)* **202**: 293–310. (doi:10.1111/j.1748-1716.2010.02246.x).
 58. Betteridge K, Arkill K, Neal C, Harper S, Foster B, Satchell S, Bates D, Salmon A. 2017 Sialic acids regulate microvessel permeability, revealed by novel *in vivo* studies of endothelial glycocalyx structure and function. *J. Physiol.* **595**, 5015–5035. (doi:10.1113/JP274167)
 59. Ray S, Kassan A, Busija AR, Rangamani P, Patel HH. 2016 The plasma membrane as a capacitor for energy and metabolism. *Am. J. Physiol. Cell Physiol.* **310**, C181–C192. (doi:10.1152/ajpcell.00087.2015)
 60. van der Laarse WJ, des Tombe AL, van Beek-Harmsen BJ, Lee-de Groot MB, Jaspers RT. 2005 Krogh's diffusion coefficient for oxygen in isolated *Xenopus* skeletal muscle fibers and rat myocardial trabeculae at maximum rates of oxygen consumption. *J. Appl. Physiol.* **99**, 2173–2180. (doi:10.1152/jappphysiol.00470.2005)
 61. Blomstrand E, Eliasson J, Karlsson HK, Köhne R. 2006 Branched-chain amino acids activate key enzymes in protein synthesis after physical exercise. *J. Nutr.* **136**, 2695–2735. (doi:10.1093/jn/136.1.2695)
 62. D'Antona G *et al.* 2010 Branched-chain amino acid supplementation promotes survival and supports cardiac and skeletal muscle mitochondrial biogenesis in middle-aged mice. *Cell Metab.* **12**, 362–372. (doi:10.1016/j.cmet.2010.08.016)
 63. Powers SK, Jackson MJ. 2008 Exercise-induced oxidative stress: cellular mechanisms and impact on muscle force production. *Physiol. Rev.* **88**, 1243–1276. (doi:10.1152/physrev.00031.2007)
 64. Powers SK, Ji LL, Kavazis AN, Jackson MJ. 2011 Reactive oxygen species: impact on skeletal muscle. *Compr. Physiol.* **1**, 941–969. (doi:10.1002/cphy.c100054)
 65. Stincone A *et al.* 2015 The return of metabolism: biochemistry and physiology of the pentose phosphate pathway. *Biol. Rev. Camb. Philos. Soc.* **90**, 927–963. (doi:10.1111/brv.12140)
 66. Levin E, Lopez-Martinez G, Fane B, Davidowitz G. 2017 Hawkmoths use nectar sugar to reduce oxidative damage from flight. *Science* **355**, 733–735. (doi:10.1126/science.aah4634)
 67. Lin J *et al.* 2004 Defects in adaptive energy metabolism with CNS-linked hyperactivity in PGC-1 α null mice. *Cell* **119**, 121–135. (doi:10.1016/j.cell.2004.09.013)
 68. Poli V. 1998 The role of C/EBP isoforms in the control of inflammatory and native immunity functions. *J. Biol. Chem.* **273**, 29 279–29 282. (doi:10.1074/jbc.273.45.29279)
 69. Litvak V, Ramsey SA, Rust AG, Zak DE, Kennedy KA, Lampano AE, Nykter M, Shmulevich I, Aderem A. 2009 Function of C/EBP δ in a regulatory circuit that discriminates between transient and persistent TLR4-induced signals. *Nat. Immunol.* **10**, 437–443. (doi:10.1038/ni.1721)
 70. Zhang L, Pan J, Dong Y, Tweardy DJ, Dong Y, Garibotto G, Mitch WE. 2013 Stat3 activation links a C/EBP δ to myostatin pathway to stimulate loss of

- muscle mass. *Cell Metab.* **18**, 368–379. (doi:10.1016/j.cmet.2013.07.012)
71. Fantin A, Vieira JM, Gestri G, Denti L, Schwarz Q, Prykhodzij S, Peri F, Wilson SW, Ruhrberg C. 2010 Tissue macrophages act as cellular chaperones for vascular anastomosis downstream of VEGF-mediated endothelial tip cell induction. *Blood* **116**, 829–840. (doi:10.1182/blood-2009-12-257832)
72. Okerblom J, Fletes W, Patel H, Schenk S, Varki A, Breen E. 2018 Data from: Human-like Cmah inactivation in mice increases running endurance and decreases muscle fatigability: implications for human evolution. Dryad Digital Repository. (<http://dx.doi.org/10.5061/dryad.qm44087>)